CERN-PRE 91-106
HEN-344/1991
(92u)

π^0 AND η MESON PRODUCTION IN π^+p AND K^+p COLLISIONS at 250 GeV/c

EHS/NA22 Collaboration

HEN-344/91
Dec. 1991

π^0 AND η MESON PRODUCTION IN π^+p AND K$^+$p COLLISIONS AT 250 GeV/c

EHS/NA22 Collaboration

M.R.Atayan[1], F.Botterweck[2], M.Charlet[2a], P.V.Chliapnikov[3], A. De Roeck[4b], E.A. De Wolf[4c], K.Dziunikowska[5d], A.M.Endler[6], Yu.V.Fisyak[7], G.V.Gevorkyan[1], D.Kisielewska[5d], W.Kittel[2], K.Olkiewicz[5d], V.M. Ronjin[3], E.K.Shabalina[7], N.A.Sotnikova[7], L.A.Tikhonova[7], O.G.Tchikilev[3], F.Verbeure[4], R. Wischnewski[8], S.A. Zotkin[7]

[1] Institute of Physics, SU-375036 Yerevan, Armenia
[2] University of Nijmegen and NIKHEF-H, NL-6525 ED Nijmegen, The Netherlands
[3] Institute for High Energy Physics, SU-142284 Protvino, Russia
[4] Inter-University Institute for High Energies, B-1050 Brussels and Dept. of Physics, Universitaire Instelling Antwerp, B-2610 Wilrijk, Belgium
[5] Institute of Physics and Nuclear Technique of Academy of Mining and Metallurgy and Institute of Nuclear Physics, PL-30055 Krakow, Poland
[6] Centro Brasileiro de Pesquisas Fisicas, Rio de Janeiro, Brasil
[7] Nucl. Phys. Institute, Moscow State University, SU-119899 Moscow, Russia
[8] Institut für Hochenergiephysik D-O-1615 Zeuthen, Germany

Abstract

We report on a study of inclusive π^0 and η meson production in π^+p and K$^+$p interactions at 250 GeV/c beam momentum. The Feynman-x spectrum of π^0 is very similar in shape and normalization to that of negatively charged particles produced in the same experiment. The results are compared with data at other energies and with FRITIOF model predictions. This model overestimates the η cross section by a factor of 2.5. It reproduces the π^0 cross section correctly, but predicts a too hard π^0 x distribution.

---

[a] EC Guest Scientist
[b] Onderzoeker IIKW, Brussels, Belgium, now at MPI München
[c] Bevoegdverklaard Navorser NFWO, Belgium
[d] Partially supported by grants from CPBP 01.06 and 01.09

1 Introduction

In this paper we present a final analysis on (forward) π^0 and η production in the inclusive reactions

$$\pi^+ + p \rightarrow \pi^0 + X, \quad (1)$$
$$K^+ + p \rightarrow \pi^0 + X, \quad (2)$$
$$\pi^+ + p \rightarrow \eta + X, \quad (3)$$
$$K^+ + p \rightarrow \eta + X; \quad (4)$$

at 250 GeV/c. The data are obtained with the European Hybrid Spectrometer (EHS) [1] using the Rapid Cycling Bubble Chamber (RCBC) as a vertex detector. The π^0's and η's are detected via the decays $\pi^0 \rightarrow \gamma\gamma$ and $\eta \rightarrow \gamma\gamma$. For γ detection the spectrometer is equipped with two gamma-detectors, intermediate (IGD) and forward (FGD) [2], with a combined acceptance allowing to study reactions (1) and (2) in the region of the Feynman variable $x \geq 0.025$ and reactions (3) and (4) in the region of $x \geq 0.10$. In addition to IGD and FGD, RCBC is used for the detection of γ's from e^+e^- pair conversion in the sensitive volume, in the range of $|x| \leq 0.3$.

The results presented here update preliminary results [3] on inclusive π^0 production in reactions (1) and (2). They are obtained on the total statistics and with a better understanding of the gamma detector performance. The results on inclusive photon production in π^+p and K^+p interactions at 250 GeV/c based on information from RCBC only can be found in [4]. Earlier studies of reactions (1) [5-14], (2) [14-16], (3) [5-6,17-20] and (4) [11,19] at other energies either suffer from low statistics or from more severe acceptance limitations.

The paper is organized as follows. In Sect.2 we describe the experimental procedure and the statistics used for the analysis. The data are presented and discussed in Sect.3 and the results are summarized in Sect.4.

2 Experimental Procedure

2.1 IGD and FGD

The details of the experimental procedure relevant to the study of inclusive π^0 and η production can be found in [3,21]. Here, we only summarize the main points.

The analysis is based on the total statistics of the two running periods of the experiment. Events are accepted for the present analysis when measured and reconstructed charge multiplicity are consistent, charge balance is satisfied, no electron is detected among the secondary tracks and the number of badly reconstructed (and therefore rejected) tracks is at most 0,1,1,2 and 3 for events with charge multiplicity 2,4,6,8 and > 8, respectively .

A further part of the events is excluded because of bad IGD or FGD data. The final samples comprise 30880 inelastic K^+p and 89474 inelastic π^+p interactions.

To maximize the signal-to-background ratio in the region of the $\pi^0(\eta)$ meson, all showers with energy $E < 0.7$ GeV in IGD and $E < 2.0$ GeV in FGD are rejected. To reduce the background still further, we reject showers originating from charged hadrons by means of the difference in lateral dimensions in IGD [3]. The rejections do not lead to a loss of the π^0 (η) signal, but reduce the background by more than 20%.

Very asymmetric π^0 and η decays are rejected by using the condition $|\cos\Theta| \leq 0.9$, where $\cos\Theta = (E_1 - E_2)/p$ with p the π^0 (η) momentum and E_1, E_2 the gamma energies.

To correct for losses due to geometrical acceptance (including the cosΘ cut described above) and conversion of γ's in RCBC and spectrometer, we assign a weight to each $\gamma\gamma$-pair using the position of the primary vertex and the beam angular characteristics. Acceptance weights are calculated for a two-dimensional grid in $(1/\gamma, \tan\alpha)$, where γ is the gamma-factor of π^0 (η) and α is the angle between π^0 (η) and beam direction in the lab system. This grid is more natural than the one used in our previous analysis [3]. There is also a weak dependence of the acceptance losses on the $\gamma\gamma$ effective mass. This dependence is taken into account by a separate simulation of the acceptance weights in the π^0 and η mass regions. The final weight assigned to each $\gamma\gamma$-pair is based on a linear interpolation between the nodes of the grid.

An additional loss of π^0's (η's) is due to the limited two-shower spatial separation in the gamma-detectors ($d = 4$ cm for FGD and 10 cm for IGD). This loss is taken into account by means of the relation $\sin\Theta^{min} \approx 2(d/L_{GD})(M/p)$, where L_{GD} is the distance from the event vertex to the gamma detector and M the $\pi^0(\eta)$ mass.

Finally, the dependence of the FGD efficiency on the γ energy has to be taken into account.

The cross section of $\pi^0(\eta)$ is obtained by fitting the $\gamma\gamma$-invariant mass distribution by the sum of a gaussian and a background of the form

$$BG(M) \;=\; \alpha_1 M^{\alpha_2} \times e^{-\alpha_3 M - \alpha_4 M^2}, \tag{5}$$

leaving the $\pi^0(\eta)$ mass and width as free parameters.

Fig.1 shows the $\gamma\gamma$-invariant mass distribution for reaction (1) in the region covered by the IGD and FGD acceptance, i.e. $x \geq 0.025$, together with the result of the fit. The FWHM of the π^0 peak is 20 MeV/c^2, consistent with the energy resolution of the γ-detectors.

2.2 RCBC photons

The details of the experimental procedure used for the detection of γ's via e^+e^- pair conversion in the sensitive volume of RCBC can be found in [4], where we have analysed γ's from RCBC in a study of direct photons. The methods described there allow to reconstruct analytically π^0's at small x from the γ x-spectrum. We are therefore able to compare the π^0 spectra in the central region from independent measurements using different detectors of EHS.

2.3 Combined GD and RCBC analysis

Combining the information on γ's from IGD and FGD with that from γ conversion in RCBC allows to study π^0 production in the total forward hemisphere of Feynman-x. For this analysis we use the selection criteria described in sect. 2.1 and in [4]. Besides GD-GD combinations the acceptance weights in this case include the probability for the detection of one γ in GD and another one in RCBC and that for both γ's in RCBC. Formally all 6 possible combinations are considered, but, in practice FGD-RCBC combinations do not contribute, RCBC-RCBC combinations are rare and excluded by efficiency cuts due to their large weights. The mixed IGD-RCBC combinations give the main contribution to π^0's produced in the region $x < 0.025$.

3 Experimental Results

3.1 Inclusive π^0 Cross Sections

The fits to the weighted inclusive $\gamma\gamma$ mass distribution using equ.(5) yield cross section values for $x \geq 0.025$ of (21.6 ± 0.6) mb for π^+p and (15.2 ± 0.8) mb for K^+p collisions, with the normalization obtained from the topological cross sections published in [21]. The errors quoted here and elsewhere in this paper (unless stated otherwise) are statistical only. The systematic uncertainty in absolute normalization is estimated to be 15%.

From the fit to the RCBC γ spectrum we obtain a cross section for $x < 0.025$ of (42±2) mb and (36±3) mb for π^+p and K^+p collisions, respectively. The inclusive π^0 cross section for all x is, therefore, estimated to be

$$\sigma(\pi^+p \to \pi^0 X) = (64 \pm 2) \text{ mb},$$

and

$$\sigma(K^+p \to \pi^0 X) = (51 \pm 3) \text{ mb}.$$

The total forward π^0 cross sections can, firstly, be obtained from an exponential extrapolation of the IGD and FGD $d\sigma/dx$ spectrum to $x = 0$. This gives $\sigma^{\pi^+p}(x \geq 0) = (38 \pm 4)$ mb and $\sigma^{K^+p}(x \geq 0) = (24 \pm 4)$ mb, where the quoted errors include uncertainties of the extrapolation.

Secondly, the same quantity may be obtained from the combination of GD data and the fit to the RCBC γ spectrum yielding (35±1) mb and (27±2) mb for π^+p and K^+p, respectively.

Thirdly, the combined IGD, FGD and RCBC analysis described in sect. 2.3 gives the values of (35±2) mb and (25±2) mb, in perfect agreement with the two other methods.

The various cross sections are summarized in Table 1.

3.2 Inclusive π^0 Feynman-x Distributions

Differential π^0 distributions are obtained by applying the fitting procedure to the $\gamma\gamma$ mass distribution in separate intervals of a given variable. The differential cross section $d\sigma/dx$ for reactions (1) and (2) obtained with IGD and FGD (for $x \geq 0.025$) is shown in Fig.2 and given in Table 2. The integrated cross section for this region agrees within errors with that obtained from fits to the integrated $\gamma\gamma$ mass distribution given in Sect.3.1.

Also shown in Fig.2 are the $d\sigma/dx$ spectra for $|x| \leq 0.3$ reconstructed from the γ spectra in RCBC. In the overlap region ($0.025 < x \leq 0.3$) the two independently obtained x-distributions agree well within errors.

In Fig.3 we present the π^0 $d\sigma/dx$ spectra as obtained from photons measured in the gamma-detectors, together with the spectra based on combined RCBC and GD data. The large errors in the region of $0.0 < x < 0.0125$ are due to the dominant contribution from mixed IGD-RCBC $\gamma\gamma$ combinations having significantly larger weights than GD-GD combinations.

In Fig.4 we compare the π^0 $d\sigma/dx$ spectra to those of positively and negatively charged particles obtained in the same experiment [23]. The shape of the π^0 distribution follows that of negatively charged particles (mostly π^-'s), but the normalization is slightly lower for π^0. This difference in normalization is smaller for π^+p than for K^+p collisions.

In Fig. 5a the Lorenz-invariant distribution

$$f(x) = \frac{2}{\sqrt{s}} \int E^* \frac{d^2\sigma}{dx dp_T^2} dp_T^2 \tag{6}$$

for reaction (1) at 250 GeV/c is compared to that for reaction $\pi^- + p \rightarrow \pi^0 + X$ at 360 GeV/c as obtained by the EHS/NA27 Collaboration [24]. The distributions agree with each other, except for the very central region, where (as expected) cross sections are slightly higher at 360 GeV/c than at 250. In Fig. 5b we show the $f(x)$ distribution for reaction (2) at 250 GeV/c together with data from a BEBC bubble chamber experiment at 70 GeV/c [16]. Within the rather large errors, the spectra at 70 GeV/c and 250 GeV/c scale.

Comparison of the π^0 $f(x)$ spectra for reactions (1) and (2) at 250 GeV/c in Fig. 5c shows that π^0 production is harder in π^+p than in K^+p collisions.

Fitting the $f(x)$ spectra by the power law dependence $f(x) \sim A(1-|x|)^n$ suggested by Dimensional Counting Rules (DCR) [25], we obtain the values for the power n as given in Table 3. Starting from $x \geq 0.3$ for reaction (1) and $x \geq 0.2$ for reaction (2), the n-values are found to be practically independent of the x-interval used in the fit. In the fragmentation region $x \geq 0.3$, the experimental values of $n = 1.7 \pm 0.1$ for reaction (1) and $n = 2.9 \pm 0.2$ for reaction (2) disagree with the DCR prediction ($n = 1.0$ for both $\pi^+ \rightarrow \pi^0$ and $K^+ \rightarrow \pi^0$ transitions). This discrepancy is perhaps not surprising since the DCR have to be applied to directly produced particles, whereas a significant fraction of observed pions originates from resonance decays. It is of interest to note that n-values for reactions (1) and (2) agree, respectively, with

the values of $n = 1.6 \pm 0.2$ for the reaction $\pi^+ p \to \pi^- X$ and $n = 2.7 \pm 0.3$ for the reaction $K^+ p \to \pi^- X$, measured in the same experiment (in the region $x \geq 0.5$) [23], while DCR predicts $n = 3.0$ for both $\pi^+ \to \pi^-$ and $K^+ \to \pi^-$ transitions.

3.3 π^0 Transverse Momentum Distributions

The transverse momentum squared distributions $d\sigma/dp_T^2$ for reactions (1) and (2) at 250 GeV/c are given in Table 4 and presented in Fig. 6. They are well described by the sum of two exponentials

$$d\sigma/dp_T^2 = ae^{-bp_T^2} + ce^{-dp_T^2} \quad , \tag{7}$$

shown as the solid lines in Fig. 6. The fitted parameter values as given in Table 5. The slope parameters (b,d) are very similar for two reactions under consideration.

3.4 Inclusive η Cross Sections

The geometrical acceptance of the gamma-detectors allows to study η production in the region $x \geq 0.1$. The addition of photons from RCBC to the analysis does not change this limitation because of the small number of mixed IGD-RCBC combinations within the η mass range contributing to the region of $0.0 < x < 0.1$. The weighted $\gamma\gamma$ invariant mass distribution for $\pi^+ p$ interactions is presented in Fig. 7a. After background subtraction (see upper right insert) a clear η meson signal is visible. A fit as described in Sect.2 gives a FWHM equal to 89 MeV/c^2, a value consistent with the experimental resolution in this mass range, and a cross section estimate of (1.9 ± 0.4) mb for $x \geq 0.1$. The η cross section for reaction (3) in this and other x-regions is given in the first column of Table 6.

In an attempt to improve the signal-to-background ratio, we have further discarded γ's forming a π^0 with any other gamma in the event. Fitting the "clean" $\gamma\gamma$ mass distributions we obtain cross sections for reaction (3) as given in the second column of Table 6. The values agree with the previous results (first column).

For reaction (4), a reasonable η signal for $x \geq 0.1$ is only obtainable in the "clean" sample (Fig. 7b). The corresponding η cross section for $x \geq 0.1$ is estimated to be (1.0 ± 0.2) mb. The cross section of reaction (4) in other x-regions is given in the third column of Table 6.

For $x \geq 0.4$ the experimental ratio $\sigma(\pi^+ p \to \eta X)/\sigma(K^+ p \to \eta X)$ equals 1.6 ± 0.5, and agrees with a maximum value of 2 expected if η is produced from (non-strange) valence quark fragmentation from the incident meson beam. Additional η-production from $\overline{s}$- valence quarks in the case of reaction (4) would lead to a ratio smaller than two. Our errors are too large to exclude this possibility.

3.5 Comparison with the FRITIOF Model

The data presented in the preceding sections are compared with the two-string FRITIOF model (version 2.0) [26], which has been shown to describe reasonably well the inclusive spectra of positively and negatively charged particles [23], as well as those of other particles [27,28] and resonances [28,29,30] in this experiment. We use the JETSET 6.3 fragmentation scheme with all parameters set to their default values, except for the following. We incorporate the tensor (2^{++}) mesons $f_2(1270)$, $a_2(1320)$ and $K_2^*(1430)$ in the ratio PS:V:T = 50:35:15 as well as their decays, take the width of the primordial transverse momentum and fragmentation transverse momentum distributions equal to 0.42 and 0.44 GeV/c, respectively, and modify the J-quark momentum distribution taken to be $f(x_J) \sim x_J(1-x_J)^{10}$ as in [28]. The FRITIOF predictions are normalized to the inelastic cross section [21].

The FRITIOF predictions for the π^0 and η inclusive cross sections in the experimentally accessible x-ranges are:

$$\sigma_{x\geq 0}(\pi^+ p \to \pi^0 X) = 35 \text{ mb}, \quad \sigma_{x\geq 0}(K^+ p \to \pi^0 X) = 25 \text{ mb},$$
$$\sigma_{x\geq 0.1}(\pi^+ p \to \eta X) = 4.0 \text{ mb}, \quad \sigma_{x\geq 0.1}(K^+ p \to \eta X) = 2.7 \text{ mb}.$$

FRITIOF overestimates the η cross section by a factor of ~ 2.5. The predicted and measured x-sections for π^0 production are in reasonable agreement for $x \geq 0$.

The model predictions for the $d\sigma/dx$ and $d\sigma/dp_T^2$ distributions in reactions (1) and (2) are compared with the data in Figs. 4 and 6. The disagreement between model and data for $d\sigma/dx$ spectra (Fig. 4) is small at small x but increases significantly at larger x. The spectrum of π^0's is much softer than predicted from π^+ and K^+ fragmentation. The π^0 spectrum is softer for K^+p interactions than for π^+p (Fig. 5c), a feature reproduced by FRITIOF (Fig. 4). The model satisfactorily describes the p_T-distributions as shown in Fig. 6. This implies that the excess of π^0's in the model is located in the region $x > 0.2$ and independent of p_T.

4 Summary and Conclusions

In this paper a study is presented of inclusive π^0 production for $x \geq 0.0$ and η production for $x \geq 0.1$ in π^+p and K$^+$p interactions at 250 GeV/c, the highest momentum available for a positive meson beam. The main results can be formulated as follows.

1. The π^0 $d\sigma/dx$ distributions in π^+p and K$^+$p reactions at 250 GeV/c differ in the forward c.m. hemisphere, thus reflecting the different quark content of the incident mesons. They are very similar in shape and in normalization to the $d\sigma/dx$ distribution of negatively charged particles in π^+p and K$^+$p reactions at 250 GeV/c, respectively.
2. Fits of the invariant $f(x)$ spectra in reactions (1) and (2) by the form $f(x) \sim A(1-x)^n$ yield values of the power n, which are not consistent with predictions from Dimensional Counting Rules.

3. Except for the central region the invariant $f(x)$ spectrum of reaction (1) at 250 GeV/c is in agreement with that of the $\pi^- p$ reaction at 360 GeV/c. The invariant $f(x)$ spectrum of reaction (2) at 250 GeV/c is in agreement with that at 70 GeV/c.
4. The FRITIOF model predicts an η cross section in reactions (3) and (4) $\sim$ 2.5 larger than measured. The integrated forward π^0 cross section is predicted correctly but the $\frac{d\sigma}{dx}$-spectrum is harder than the measured one.

Acknowledgments.

It is a pleasure to thank the EHS coordinator L.Montanet, the operating crews and staff of EHS, SPS and H2 beam, as well as the scanning and processing teams of our laboratories for their invaluable help in this experiment. We are also grateful to our colleagues from the III.Physikalisches Institut B, RWTH, Aachen, Germany, from the Department of High Energy Physics of Helsinki University, Finland and from the Institute of Nuclear Problems and University of Warsaw, Poland, for early contributions to this experiment.

References

[1] M. Aguilar-Benitez et al.: Nucl. Instrum. Methods 205 (1983) 79
[2] B. Powell et al.: Nucl. Instrum. Methods 198 (1982) 217
[3] I. V.Ajinenko et al. (NA22): Z. Phys. C - Particles and Fields 35 (1987) 7
[4] F. Botterweck et al. (NA22): Z. Phys. C - Particles and Fields 51 (1991) 541
[5] J. Guy et al.: Nucl. Phys. B155 (1979) 320
[6] J. Elliott et al.: Nucl. Phys. B133 (1978) 1
[7] K. Böckmann et al.: Nucl. Phys. B119 (1977) 253
[8] N.N. Biswas et al.: Phys. Rev. D10 (1974) 3579
[9] I.V. Ajinenko et al.: Sov. J. Nucl. Phys. 31 (1980) 62
[10] M. Alston-Garnjost et al.: Phys. Rev. Lett. 35 (1975) 142
[11] a) A.V. Barnes et al.: Nucl. Phys. B145 (1978) 45;
b) R.G. Kennett et al.: Nucl. Phys. B177 (1981) 1;
c) R.G. Kennett: Ph.D. Thesis, "Experimental tests of triple Regge theory", CALT-68-472(1979)
[12] J. Elliott et al.: Phys. Rev. D17 (1978) 83
[13] R. Apsimon et al.: Z. Phys. C - Particles and Fields 52 (1991) 397
[14] J. Bartke et. aL.: Acta Phys. Pol. B5 (1974) 689
[15] I.V. Ajinenko et al.: Nucl. Phys. B162 (1980) 61
[16] M. Barth et al.: Z. Phys. C - Particles and Fields 22 (1984) 23
[17] G.S. Bitsadze et al.: Nucl. Phys. B279 (1987) 770
[18] M.Bonesini et al.: Z. Phys. C - Particles and Fields 42 (1989) 527
[19] a) G.J. Donaldson et al.: Phys. Rev. Lett 40 (1978) 684;
b) A.V. Barnes et al.: Phys. Rev. Lett 41 (1978) 1260
[20] H. Kirk et al.: Nucl. Phys. B128 (1977) 379
[21] M. Adamus et al. (NA22): Z. Phys. C - Particles and Fields 32 (1986) 475
[22] J.R. Elliot et al.: Phys. Rev. D17 (1978) 83
P.V. Chliapnikov et al.: Phys. Lett. B141 (1984) 276
[23] M. Adamus et al. (NA22): Z. Phys. C - Particles and Fields 39 (1988) 311
[24] M. Aguilar-Benitez et al. (NA27): Z. Phys. C - Particles and Fields 34 (1987) 419
[25] J.F. Gunion: Phys. Lett. 88B (1979) 150
[26] B. Andersson, G. Gustafson, B. Nilsson-Almqvist: Nucl. Phys. B281 (1987) 289
[27] I.V. Ajinenko et al. (NA22): Z. Phys. C - Particles and Fields 46 (1990) 525
[28] I.V. Ajinenko et al. (NA22): Z. Phys. C - Particles and Fields 44 (1990) 573
[29] N.M. Agababyan et al. (NA22): Z. Phys. C - Particles and Fields 41 (1989) 539
[30] N.M.Agababyan et al. (NA22): Z. Phys. C - Particles and Fields 46 (1990) 387

Table 1. Integrated cross sections of inclusive π^0 production in reactions $\pi^+p \rightarrow \pi^0 + X$ and $K^+p \rightarrow \pi^0 + X$ at 250 GeV/c determined

a) from $\gamma\gamma$-invariant mass distributions of photons measured in the EHS gamma-detectors IGD and FGD,

b) from γ-conversions observed in the Rapid Cycling Bubble Chamber using the π^0 reconstruction method of ref.[4],

c) like a) but extrapolated to $x = 0$,

d) from $\gamma\gamma$-invariant mass distributions of photons measured in IGD, FGD and γ-conversions observed in the RCBC.

	Device	π^+p	K^+p
$\sigma(x \geq 0.025)$ [a)]	IGD + FGD	21.6±0.6	15.2±0.8
$\sigma(x \geq 0.025)$	FRITIOF	28	17
$\sigma(x \leq 0.025)$ [b)]	RCBC	42±2	36±3
σ(all x)	all	64±2	51±3
σ(all x)	FRITIOF	73	56
$\sigma(x \geq 0)$ [c)]	IGD + FGD	38±4	24±4
$\sigma(x \geq 0)$ [b)]	all	35±1	27±2
$\sigma(x \geq 0)$ [d)]	all	35±2	25±2
$\sigma(x \geq 0)$	FRITIOF	35	25

Table 2: $d\sigma/dx$ and $f(x)$ distributions for reactions (1) and (2) at 250 GeV/c

	Reaction	$\pi^+p \to \pi^0 + X$		$K^+p \to \pi^0 + X$	
	x-interval	$d\sigma/dx$(mb)	$f(x)$(mb)	$d\sigma/dx$(mb)	$f(x)$(mb)
Combined	0.000 ÷ 0.0125	680 ± 140	19 ± 4	480 ± 170	—
GD-RCBC	0.0125 ÷ 0.025	435 ± 29	15 ± 1	348 ± 32	13 ± 1
GD only	0.025 ÷ 0.05	297 ± 16	15 ± 1	205 ± 23	11 ± 1
	0.05 ÷ 0.075	143 ± 9	13 ± 1	123 ± 12	10 ± 1
	0.075 ÷ 0.1	100 ± 6	10 ± 1	82 ± 9	8.1 ± 0.9
	0.1 ÷ 0.125	57 ± 4	7.2 ± 0.6	54 ± 5	6.5 ± 0.6
	0.125 ÷ 0.15	54 ± 4	7.7 ± 0.5	35 ± 4	5.2 ± 0.6
	0.15 ÷ 0.175	32 ± 3	5.8 ± 0.5	22 ± 4	4.3 ± 0.7
	0.175 ÷ 0.2	31 ± 2	5.7 ± 0.4	19 ± 3	4.5 ± 0.6
	0.2 ÷ 0.25	23 ± 2	5.4 ± 0.3	14 ± 1	3.3 ± 0.3
	0.25 ÷ 0.3	17 ± 1	4.5 ± 0.3	11 ± 1	2.6 ± 0.3
	0.3 ÷ 0.35	11 ± 0.6	3.5 ± 0.2	4.4 ± 0.7	2.0 ± 0.3
	0.35 ÷ 0.4	6.6 ± 0.6	2.4 ± 0.2	3.8 ± 0.9	1.8 ± 0.2
	0.4 ÷ 0.5	4.8 ± 0.4	2.2 ± 0.2	2.5 ± 0.5	1.3 ± 0.1
	0.5 ÷ 0.6	2.5 ± 0.2	1.3 ± 0.1	1.4 ± 0.3	0.88 ± 0.13
	0.6 ÷ 0.7	1.5 ± 0.2	1.0 ± 0.1	0.3 ± 0.1	0.21 ± 0.12
	0.7 ÷ 0.8	0.90 ± 0.20	0.72 ± 0.13	0.2 ± 0.1	0.09 ± 0.06
	0.8 ÷ 0.9	0.22 ± 0.06	0.19 ± 0.05	0.03 ± 0.02	0.03 ± 0.03
	0.9 ÷ 1.0	0.09 ± 0.06	0.08 ± 0.07		
	$\int \frac{d\sigma}{dx} dx(mb)(x \geq 0.025)$	21.7 ± 0.5		15.6 ± 0.7	

Table 3. Power n obtained from the fit of the π^0 $f(x)$ distribution for reactions (1) and (2) at 250 GeV/c by the form $f(x) = A(1-|x|)^n$ in the indicated x-ranges

n	$x \geq 0.2$	$x \geq 0.3$	$x \geq 0.4$	$x \geq 0.5$	$x \geq 0.6$
π^+p	2.1 ± 0.1	1.7 ± 0.1	1.6 ± 0.1	1.5 ± 0.2	1.6 ± 0.2
χ^2/NDF	26/8	10/6	5/4	4/3	2.6/2
K$^+$p	2.9 ± 0.2	2.9 ± 0.3	3.0 ± 0.4		
χ^2/NDF	4/7	4/5	2.6/3		

Table 4. $d\sigma/dp_T^2$ distributions for reactions (1) and (2) at 250 GeV/c in the interval $x \geq 0.025$

p_T^2-interval	$d\sigma/dp_T^2$ mb/(GeV/c)$^{-2}$	
(GeV/c)^2	π^+p	K$^+$p
0.00 ÷ 0.02	141 ± 22	87 ± 18
0.02 ÷ 0.04	99 ± 12	76 ± 15
0.04 ÷ 0.08	95 ± 6	75 ± 7
0.08 ÷ 0.12	75 ± 5	57 ± 6
0.12 ÷ 0.16	50 ± 3	30 ± 4
0.16 ÷ 0.20	33 ± 2	31 ± 3
0.20 ÷ 0.25	27 ± 1	19 ± 2
0.25 ÷ 0.30	20 ± 1	18 ± 2
0.30 ÷ 0.35	19 ± 1	13 ± 1
0.35 ÷ 0.40	16 ± 1	10 ± 1
0.40 ÷ 0.45	10 ± 0.6	8.3 ± 1.9
0.45 ÷ 0.50	8.3 ± 0.6	7.0 ± 0.7
0.50 ÷ 0.60	6.4 ± 0.4	3.1 ± 0.4
0.60 ÷ 0.70	3.8 ± 0.3	2.4 ± 0.3
0.70 ÷ 0.80	2.7 ± 0.2	2.0 ± 0.3
0.80 ÷ 0.90	2.4 ± 0.3	1.5 ± 0.2
0.90 ÷ 1.00	1.5 ± 0.2	0.66 ± 0.13
1.00 ÷ 1.50	0.74 ± 0.04	0.49 ± 0.05
1.50 ÷ 2.00	0.28 ± 0.02	0.13 ± 0.03
2.00 ÷ 2.50	0.15 ± 0.02	0.06 ± 0.02
$\int \frac{d\sigma}{dp_T^2} dp_T^2$(mb)	22.2 ± 0.6	16.1 ± 0.7

Table 5. Fits of $d\sigma/dp_T^2$ distributions in reactions (1) and (2) at 250 GeV/c to the form $ae^{-bp_T^2} + ce^{-dp_T^2}$ in the interval $x \geq 0.025$

BReaction	p_T^2-interval	a	c	b	d	χ^2/NDF
	$(\mathrm{GeV/c})^2$	$\mathrm{mb/(GeV/c)^2}$		$(\mathrm{GeV/c})^{-2}$		
π^+p	0.0 ÷ 2.5	110 ± 7	8 ± 3	6.6 ± 0.6	1.9 ± 0.3	33/16
K$^+$p	0.0 ÷ 2.5	90 ± 7	7 ± 2	6.9 ± 0.5	2.2 ± 0.2	29/16

Table 6. Inclusive η cross section in reactions (3) and (4) at 250 GeV/c in different x-regions

	Cross section (mb)		
x region	π^+p		K$^+$p
	"Raw" sample	"Clean" sample	"Clean" sample
$x \geq 0.1$	1.9 ± 0.4	1.7 ± 0.3	1.0 ± 0.2
$x \geq 0.2$	1.0 ± 0.3	0.9 ± 0.2	0.5 ± 0.1
$x \geq 0.4$	0.5 ± 0.1	0.47 ± 0.07	0.29 ± 0.07
$x \geq 0.5$	0.41 ± 0.09	0.39 ± 0.07	0.24 ± 0.05

Figure captions

Fig.1: Weighted $\gamma\gamma$ invariant mass distribution with $x(\gamma\gamma) \geq 0.025$ for π^+p interactions at 250 GeV/c. The curves show the result of the fit described in the text

Fig.2: The $d\sigma/dx$ distribution obtained from IGD and FGD $\gamma\gamma$ invariant mass spectra in separate x-intervals (full circles), compared to the result of a fit to the RCBC γ spectrum (open circles) **(a)** for π^+p interactions at 250 GeV/c, **(b)** for K^+p interactions at 250 GeV/c

Fig.3: The $d\sigma/dx$ distribution obtained from IGD and FGD $\gamma\gamma$ invariant mass spectra (full circles), compared with the spectrum based on combined RCBC and GD data (open circles) **(a)** for π^+p interactions at 250 GeV/c, **(b)** for K^+p interactions at 250 GeV/c

Fig.4: The $d\sigma/dx$ distribution compared with the prediction of the FRITIOF model (dashed-dotted curve) and the corresponding data for reactions $\pi^+p \rightarrow C^+ + X$ and $\pi^+p \rightarrow C^- + X$ at 250 GeV/c [22] **(a)** for π^+p interactions at 250 GeV/c, **(b)** for K^+p interactions at 250 GeV/c

Fig.5: The invariant $f(x)$ distributions for **(a)** π^+p at 250 GeV/c and π^-p at 360 GeV/c [23]; **(b)** K^+p at 70 [16] and 250 GeV/c; **(c)** π^+p and K^+p at 250 GeV/c

Fig.6: The $d\sigma/dp_T^2$ distribution for reactions (1)**(a)** and (2)**(b)** with $x \geq 0.025$ at 250 GeV/c. Solid curves are fits to the sum of two exponentials described in the text. Dashed-dotted curves are predictions of the FRITIOF model

Fig.7: **(a)** Weighted $\gamma\gamma$ invariant mass distribution in the region $x(\gamma\gamma) \geq 0.1$ for π^+p interactions at 250 GeV/c. The curves are the result of the fit described in the text. The insert shows the signal after subtraction of the background; **(b)** the same as in Fig. 7a, but for K^+p interactions at 250 GeV/c and after removal of photons also contributing to the π^0-signal

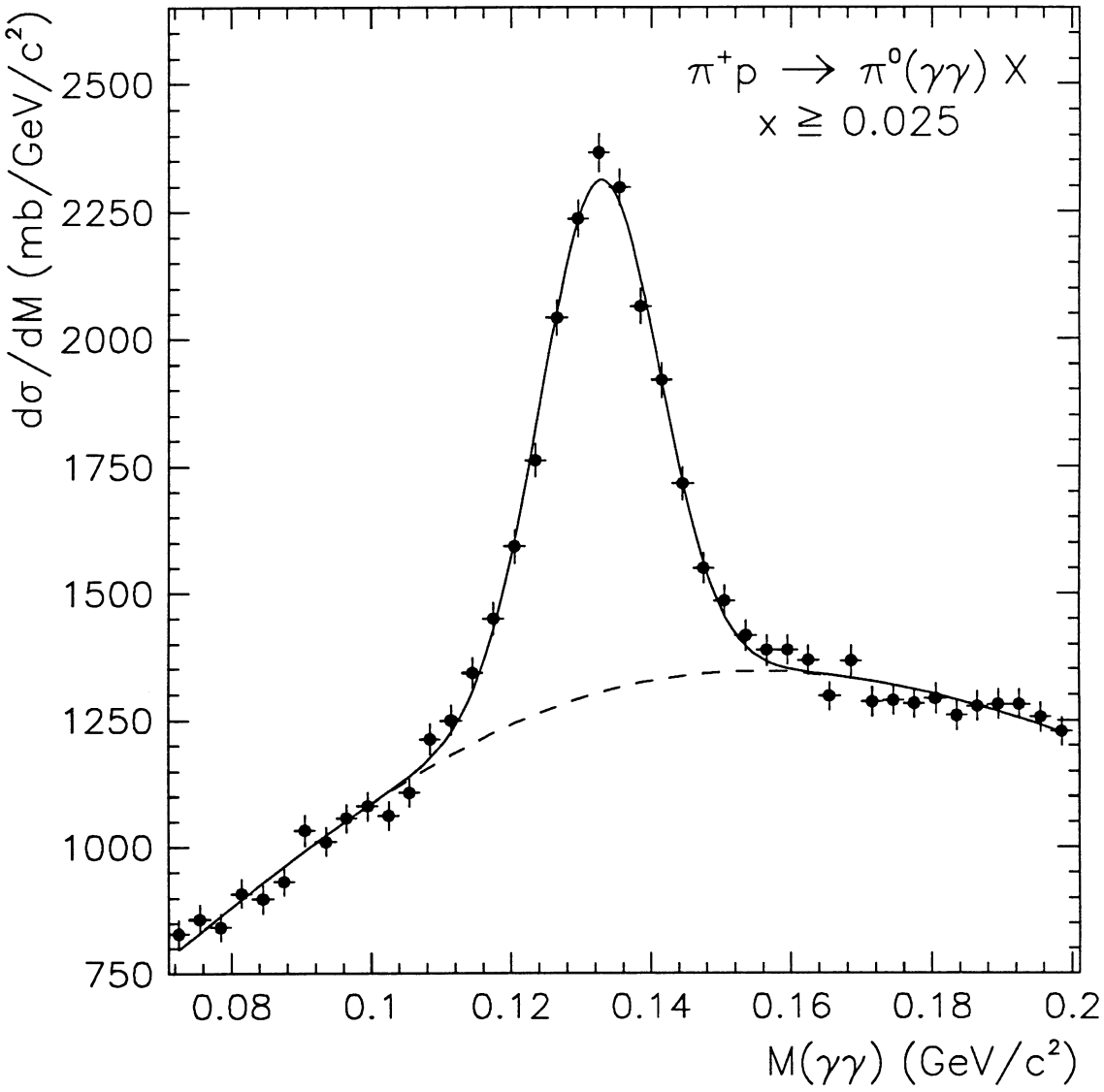
$\pi^+ p \rightarrow \pi^0(\gamma\gamma)\, X$
$x \geqq 0.025$
$d\sigma/dM$ (mb/GeV/c^2)
2500
2250
2000
1750
1500
1250
1000
750
0.08
0.1
0.12
0.14
0.16
0.18
0.2
$M(\gamma\gamma)$ (GeV/c^2)

Fig. 1

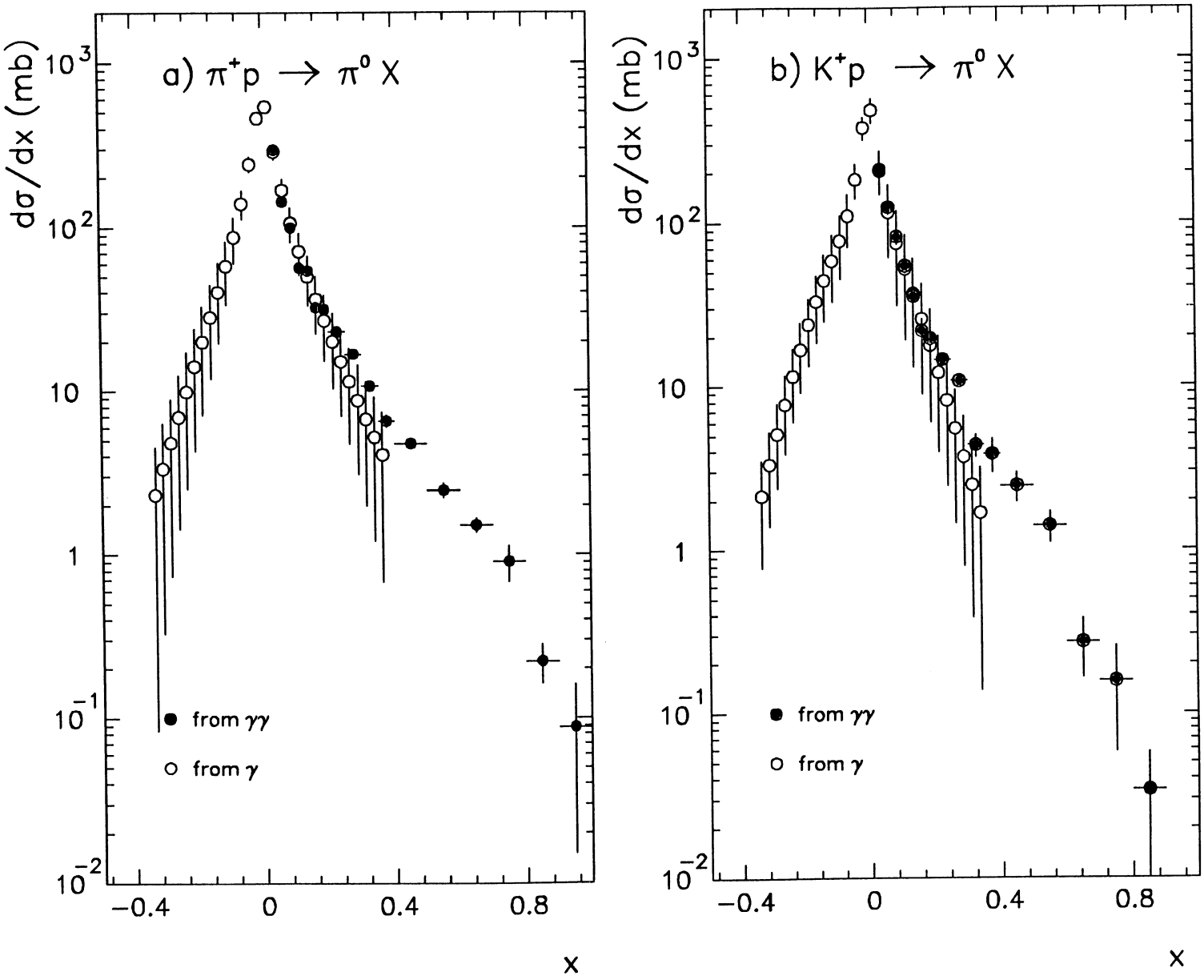
a) $\pi^+ p \rightarrow \pi^0 X$
b) $K^+ p \rightarrow \pi^0 X$
$d\sigma/dx$ (mb)
10^3
10^2
10
1
10^{-1}
10^{-2}
−0.4
0
0.4
0.8
x
from $\gamma\gamma$
from γ

FIG. 2

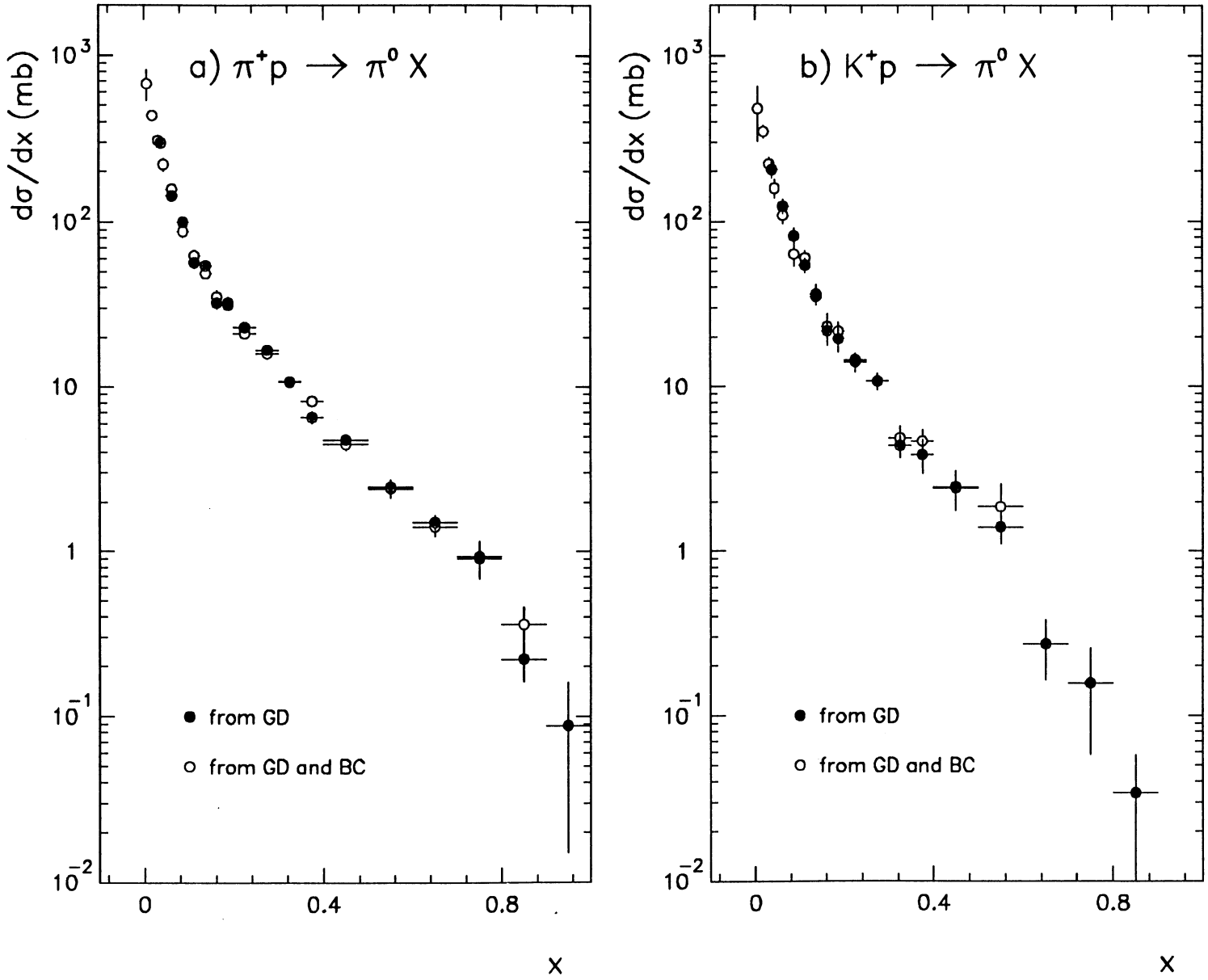
a) $\pi^+ p \rightarrow \pi^0 X$
b) $K^+ p \rightarrow \pi^0 X$
$d\sigma/dx$ (mb)
10^3
10^2
10
1
10^{-1}
10^{-2}
0
0.4
0.8
x
from GD
from GD and BC

FIG. 3

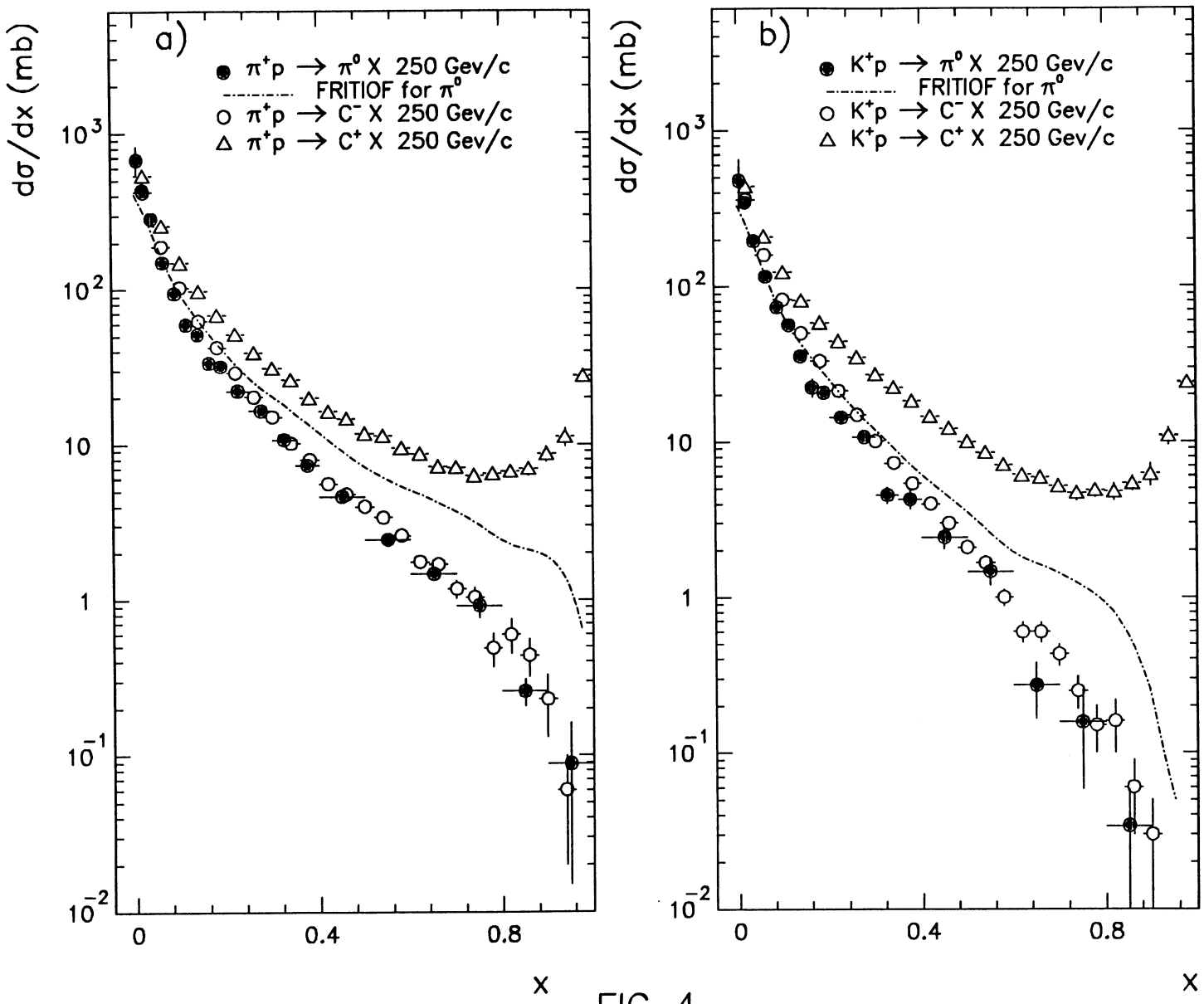
a)
$\pi^+p \rightarrow \pi^0 X$ 250 Gev/c
FRITIOF for π^0
$\pi^+p \rightarrow C^- X$ 250 Gev/c
$\pi^+p \rightarrow C^+ X$ 250 Gev/c
$d\sigma/dx$ (mb)
10^3
10^2
10
1
10^{-1}
10^{-2}
0
0.4
0.8
x
b)
$K^+p \rightarrow \pi^0 X$ 250 Gev/c
FRITIOF for π^0
$K^+p \rightarrow C^- X$ 250 Gev/c
$K^+p \rightarrow C^+ X$ 250 Gev/c
$d\sigma/dx$ (mb)
10^3
10^2
10
1
10^{-1}
10^{-2}
0
0.4
0.8
x

FIG. 4

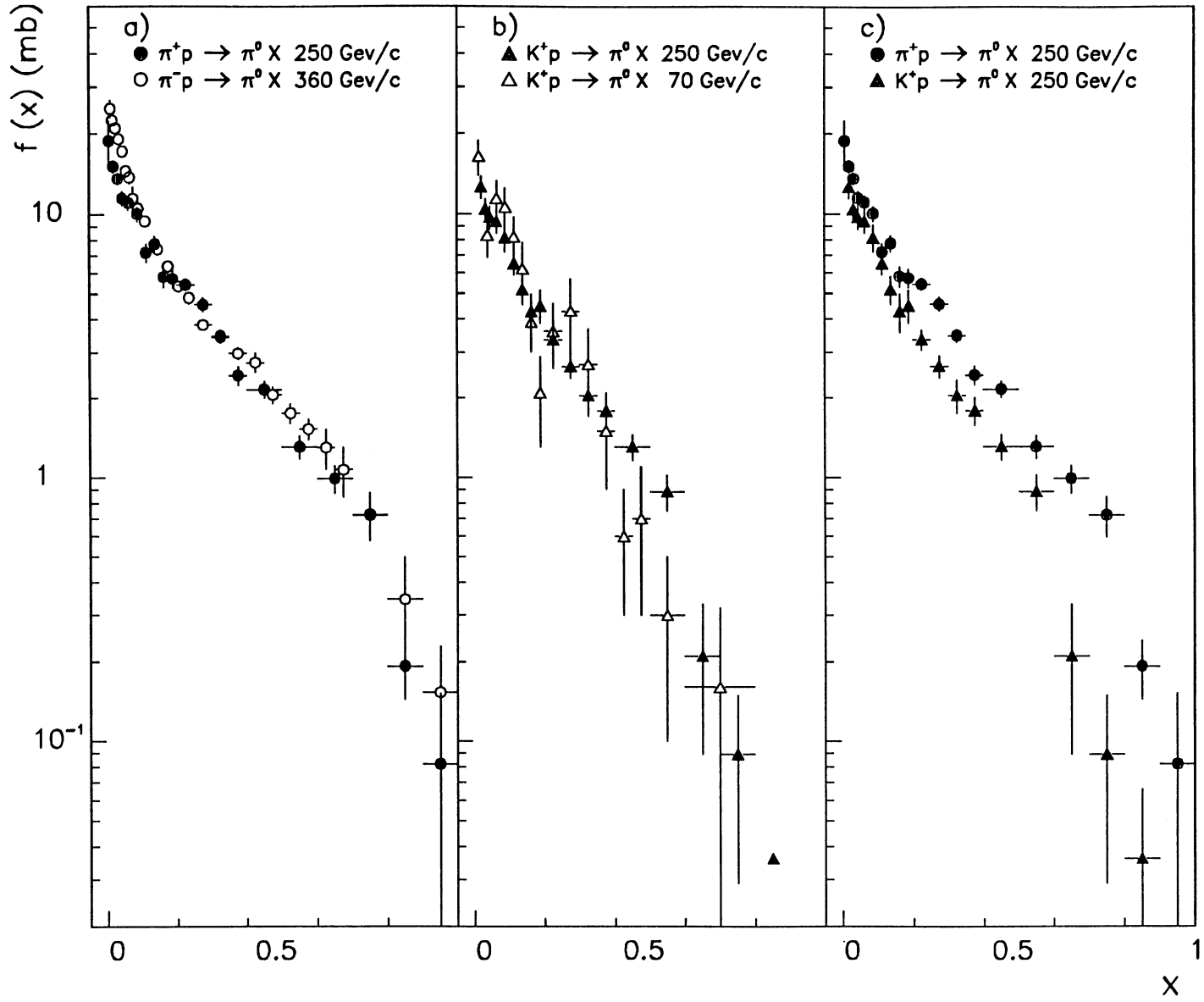
a)
● $\pi^+p \rightarrow \pi^0 X$ 250 Gev/c
○ $\pi^-p \rightarrow \pi^0 X$ 360 Gev/c
b)
▲ $K^+p \rightarrow \pi^0 X$ 250 Gev/c
△ $K^+p \rightarrow \pi^0 X$ 70 Gev/c
c)
● $\pi^+p \rightarrow \pi^0 X$ 250 Gev/c
▲ $K^+p \rightarrow \pi^0 X$ 250 Gev/c
f (x) (mb)
10
1
10^{-1}
0
0.5
0
0.5
0
0.5
1
X

FIG. 5

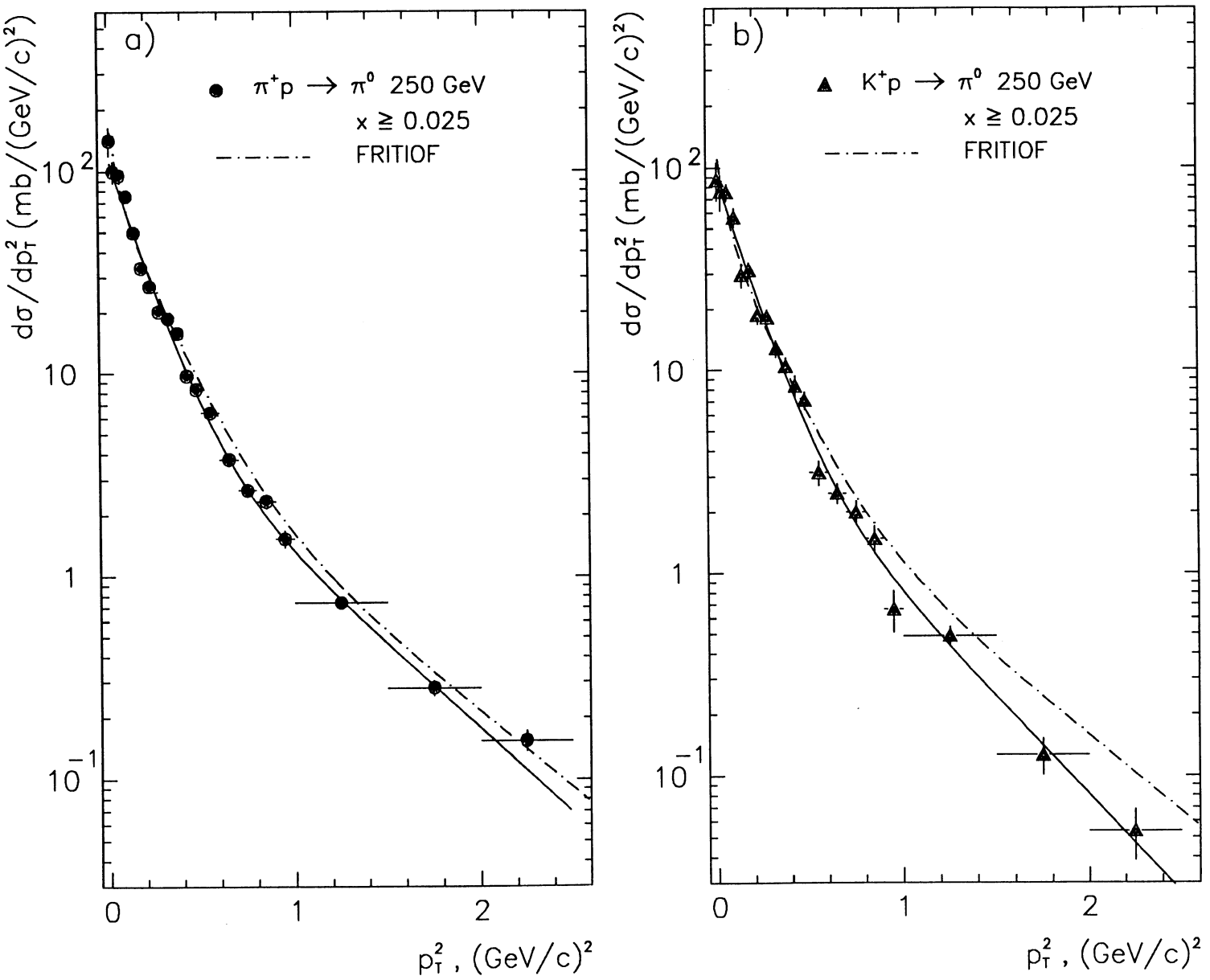
a)
$\pi^+ p \rightarrow \pi^0$ 250 GeV
$x \geq 0.025$
FRITIOF
$d\sigma/dp_T^2$ (mb/(GeV/c)^2)
10^2
10
1
10^{-1}
0
1
2
p_T^2, (GeV/c)^2
b)
$K^+ p \rightarrow \pi^0$ 250 GeV
$x \geq 0.025$
FRITIOF
$d\sigma/dp_T^2$ (mb/(GeV/c)^2)
10^2
10
1
10^{-1}
0
1
2
p_T^2, (GeV/c)^2

Fig. 6

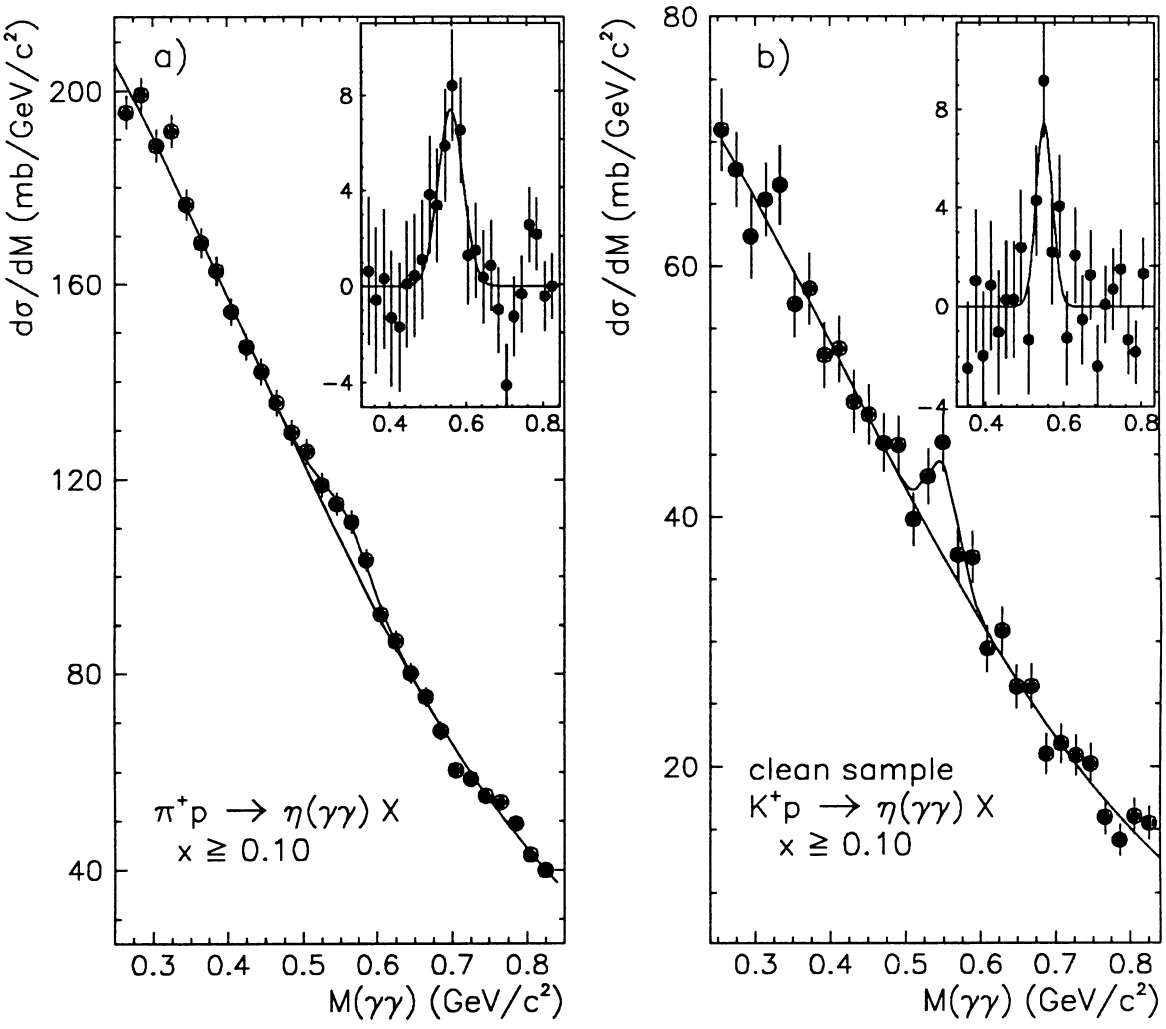
a)
b)
dσ/dM (mb/GeV/c²)
M(γγ) (GeV/c²)
π⁺p → η(γγ) X
x ≧ 0.10
K⁺p → η(γγ) X
x ≧ 0.10
clean sample

Fig. 7